Smart Structures and Systems, *Vol. 32, No. 2 (2023) 83-99*
https://doi.org/10.12989/sss.2023.32.2.083

Temperature distribution prediction in longitudinal ballastless slab track with various neural network methods

Hanlin Liu [1,3], Wenhao Yuan [2], Rui Zhou*[2,3], Yanliang Du [2], Jingmang Xu [3] and Rong Chen [3]

[1] *Mining College, Guizhou University, Guiyang, Guizhou Province, China*
[2] *School of Civil Engineering & Traffic Engineering, Shenzhen University, Shenzhen, Guangdong Province, China*
[3] *MOE Key Laboratory of High-Speed, Railway Engineering, Southwest Jiaotong University, Chengdu, Sichuan Province, China*

(*Received April 10, 2023, Revised July 13, 2023, Accepted August 15, 2023*)

Abstract. The temperature prediction approaches of three important locations in an operational longitudinal slab track-bridge structure by using three typical neural network methods based on the field measuring platform of four meteorological factors and internal temperature. The measurement experiment of four meteorological factors (e.g., ambient temperature, solar radiation, wind speed, and humidity) temperature in the three locations of the longitudinal slab and base plate of three important locations (e.g., mid-span, beam end, and Wide-Narrow Joint) were conducted, and then their characteristics were analyzed, respectively. Furthermore, temperature prediction effects of three locations under five various meteorological conditions are tested by using three neural network methods, respectively, including the Artificial Neural Network (ANN), the Long Short-Term Memory (LSTM), and the Convolutional Neural Network (CNN). More importantly, the predicted effects of solar radiation in four meteorological factors could be identified with three indicators (e.g., Root Means Square Error, Mean Absolute Error, Correlation Coefficient of R2). In addition, the LSTM method shows the best performance, while the CNN method has the best prediction effect by only considering a single meteorological factor.

Keywords: ballastless track-bridge structure; field measuring platform; meteorological factors; neural network methods; temperature prediction

1. Introduction

In the past decades, the longitudinal ballastless track in high-speed railway were constructed in more and more distinguished railways over all the world, due to their high stability, durability, and low maintenance (Ren *et al*. 2021). Most of the longitudinal slab tracks are built on the viaduct to ensure the standard maximum grade of the line, and the simply-support concrete box girder with a span of 32 m is the primary bridge structure at current, for example, there are 87.7% (about 175.4 km) of the bridge foundation in the famous Beijing-Tianjin Inter-city Railway (Su *et al*. 2019). The Beam End, Mid-Span, and Wide-Narrow Joint are important locations in the ballastless track-bridge structure since they are the key force-transfer parts when the loads act on the track structure (Zhao *et al*. 2021). In order to improve the long-term operational safety, the structural damage of longitudinal slab track-bridge structure should be accurately evaluated, especially for the Beam End, Mid-Span, and Wide-Narrow Joint.

The temperature gradient in the longitudinal slab track is an important characteristic impact on the ballastless track-bridge structure, which could lead to huge thermal stress accumulation inside the track slab (Guo *et al*. 2022, Zhou *et al*. 2023a, 2021). The temperature field is mainly governed by meteorological factors with respect to Ambient Temperature (AT), Solar Radiation (SR), Wind Speed (WS), Relative Humidity (RH) (Cai *et al*. 2019, Lu and Wang 2023). In order to reveal the heat transfer mechanism of the slab track under various meteorological factors, Yang *et al*. (2017), and Zhou *et al*. (2023a) established the transient analysis of heat transfer models of the longitudinal slab track and found that the stronger solar radiation and the higher ambient temperature are the main factors causing the internal higher temperature of the track, especially when the thermal contrast of the ambient temperature is higher than 0.5°C. In addition, Zhou *et al*. (2022b) studied the thermal effect of CRTS II slab track under various environmental temperatures conditions using the huge environmental testing chamber and found the heat transfer principles of multi-layer concrete structures under different environmental temperatures conditions (Zhou *et al*. 2022b, 2023b). However, these meteorological factors are highly dependent on the site-specific conditions and cannot be easily generalized, which leads to an obvious temperature gradient in the longitudinal slab track not easily predicted by the heat conduction equations (Zhang *et al*. 2022, Zumin and Fujian 2014). Based on the monitoring field data, many scholars studied the internal temperature characteristics of the longitudinal slab track and the relationship between track slab surface temperature and ambient temperature by using various statistical methods, for example, the nonlinear regression method (Lou *et al*. 2018, Yu *et al*. 2020), a quartic polynomial and exponential distribution model (Xu

*Corresponding author, Ph.D., Associate Professor,
E-mail: zhourui@szu.edu.cn

ISSN: 1738-1584 (Print), 1738-1991 (Online)

et al. 2022, Liu *et al*. 2023), Fourier series function (Dai and Su 2016, Dai *et al*. 2018). Their results reveal the nonlinear distribution of temperature gradient and the correlation relationship between the internal temperature and specific external factors by fitting equations. However, the correlation relationship among these meteorological factors become more complex due to global warming, which poses great challenges for traditional statistical methods to effectively predict the internal temperature field in track structures subjected to various meteorological factors (Dai *et al*. 2022, Xin *et al*. 2022). Therefore, it is of great importance to explore a high-efficiency data-driven method to accurately predict the temperature field in longitudinal track-bridge structures under various meteorological conditions.

Based on the field monitoring data, some basic machine learning algorithms are used to predict the temperature field in longitudinal ballastless track structures in recent years. Guo *et al*. (2018) established the fore-warning model of track temperature gradient classification based on the support vector machine and calculated the warming threshold of themeteorological parameters. Xin *et al*. (2022) developed a hybrid convolutional neural network-support vector machine (CNN-SVM) approach to explore the relationship between the structural thermal characteristics and interfacial properties. The predicted accuracy in the 0.65 m length mortar void conditions is higher than 90%. Ma and Gao (2021) proposed a hybrid model integrating traditional and machine learning models, including the wavelet transform, convolutional neural network, and long-term memory. The proposed model perfectly captures the nonlinear characteristics based on three indicators of average Root Means Square Error (RMSE), Mean Absolute Error (MAE), and Pearson Correlation Coefficients (PCC). Furthermore, Shi *et al*. (2022) predict the vertical temperature gradient of the track slab with various machine-learning techniques due to solar radiation. It is found that the categorical boosting-based hybrid approach has the best prediction performance. Furthermore, compared with various machine learning methods, deep learning methods have a higher accuracy rate to predict the temperature field in the track-bridge structures (Shi *et al*. 2022, Wang *et al*. 2021, Zhang *et al*. 2020a). In addition, the Recurrent Neural Network (RNN), the Artificial Neural Network (ANN), and the Convolutional Neural Network (CNN) are the three basic types of deep learning methods in data-driven prediction based on a great deal of monitoring data. CNN and ANN are designed for exploring the spatial correlation and hidden features from tons of collected data. The Long Short-term Memory (LSTM) is typical of RNN, which is designed for mining the long-term temporal correlation in monitoring data. However, they predict the effect of the temperature field in track-bridge structure by using these popular different neural network methods subjected to various meteorological factors that should be further tested.

Since the internal temperature field of a ballastless track could be affected by many factors, such as meteorological factors, geographical factors, material factors, etc. Only the effects of meteorological factors on internal temperature are investigated in this paper. This paper aims at evaluating the performance of three typical data-driven prediction approaches to internal temperature in ballastless track-bridge structures under various meteorological conditions. Firstly, the field platform of an automatic small weather station and temperature sensors installed in a longitudinal ballastless slab track-bridge structure were introduced, and the temperature prediction models of three neural network methods are established. Secondly, the characteristics of four meteorological factors and internal temperature are analyzed, respectively. Finally, the prediction effects of internal temperature of three important locations under various meteorological conditions are compared by using three neural network methods. The present study could help improve the evaluation thermal performance of the ballastless track to guarantee line safety of China's high-speed railway in long-term operation.

2. Methodology

The temperature prediction approach in ballastless track-bridge structures under various meteorological conditions includes the following steps: (1) establishing a long-term field online measured platform to collect real-time data on four meteorological and internal temperatures; (2) analyzing the characteristics of four meteorological factors (AT, SR, WS, RH) and internal ballastless temperature of track slab and base plate, as well as their correlation relationship; (3) enrolling the predictive models of three neural network methods, including the ANN, LSTM, and CNN; (4) validating three predict models through the special training and testing date, after the data collection and preprocessing; (5) comparing the predict effects of the internal temperature of three important locations (e.g., midspan, beam end, and wide-narrow joint)

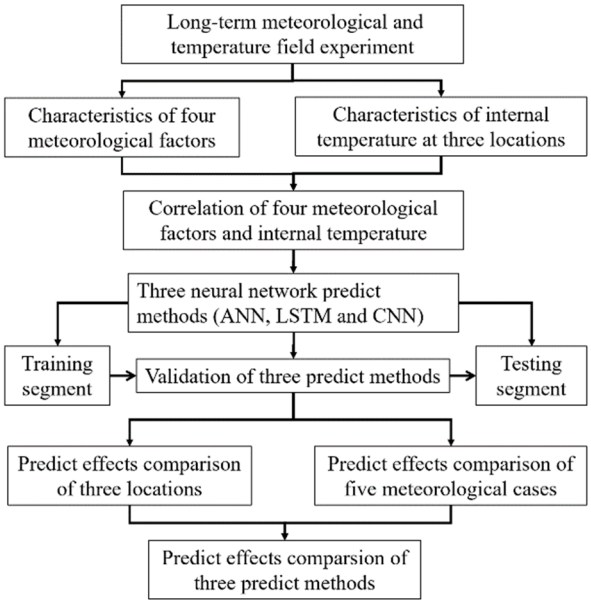

Fig. 1 Calculation flow of the temperature prediction approach

Table 1 Meteorological parameters of the automobile small weather station

Meteorological parameters	Measurement range	Resolution ratio	Accuracy
Ambient temperature	-50-100℃	0.1℃	±0.5℃
Wind speed	1-67 m/s	0.1 m/s	+5%
Wind direction	0-360°	1°	+7°
Relative humidity	1~100%	1%	+3~4%
Rainfall	0-7 mm/min	0.2 mm	+4%
Solar radiation	0-1800 W/m^2	1 W/m^2	+5%

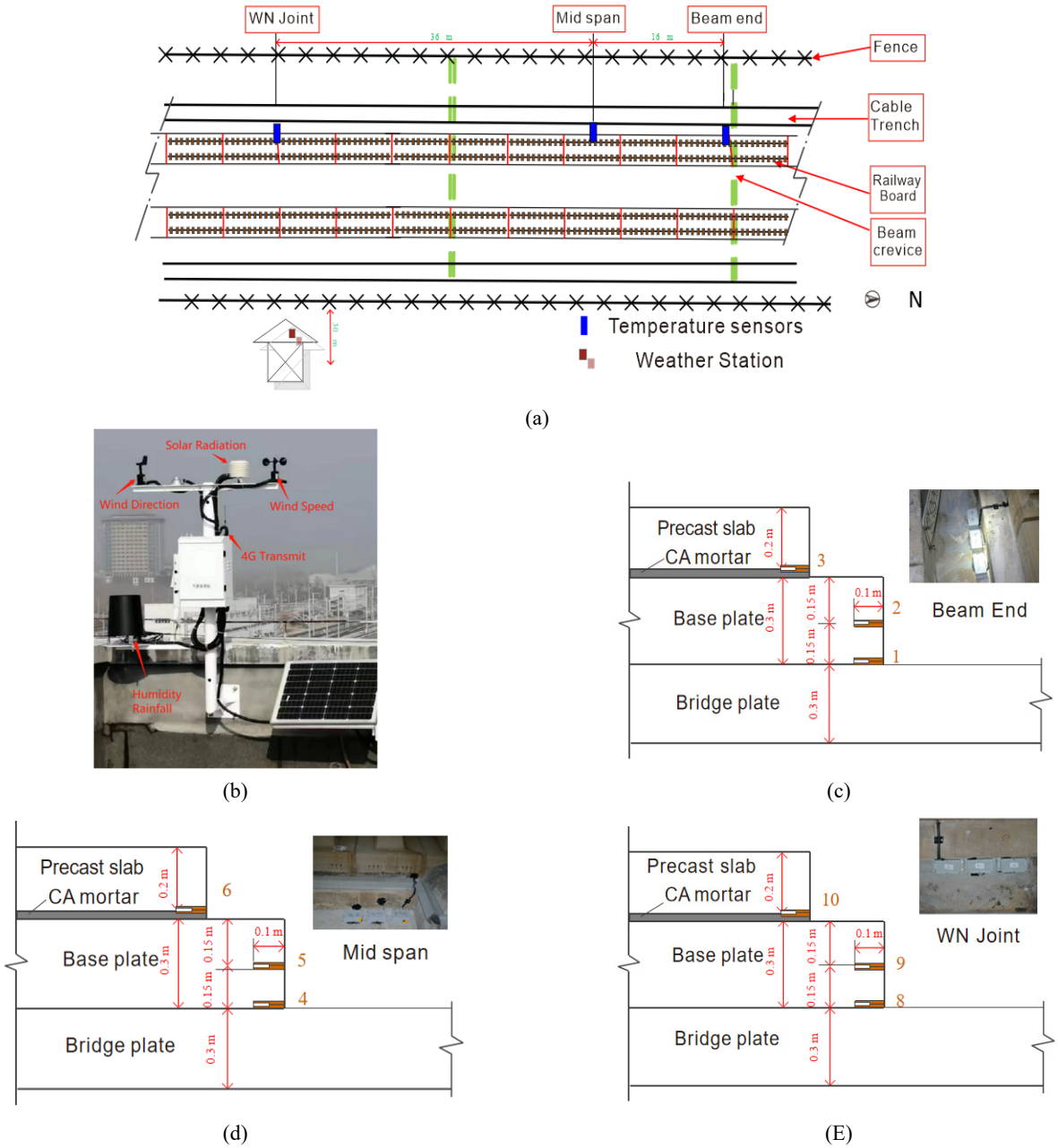

Fig. 2 The detailed installation of the automobile weather station and internal temperature sensors. (a) the measured three locations of long-term meteorological and temperature field platforms. (b) the equipment of a weather station; (c) three temperature sensors installed at the Beam End; (d) three temperature sensors installed at the Mid Span; (e) three temperature sensors installed at WN Joint

under five different meteorological conditions, as well as the predict effects of the internal temperature by using three neural network methods. The calculation flow of the temperature prediction approach is drawn in Fig. 1.

2.1 Measurement experiment tests

The experimental area of Shandong section was selected in the Beijing-Shanghai high-speed railway (BSHSR). The BSHSR is finished in 2011 and designed with a typical longitudinal slab ballastless track in China. Also, the long-term meteorological and temperature real-time monitoring device was set up near the line with a distance of 50 m. As described in Fig. 2(a), an automobile weather station of the Vantage Pro2 from DAVIS manufacturer (Fig. 2(b)) was utilized for real-time, remote, and continuous monitoring of the meteorological factors (AT, SR, WS, RH). The measurement indicators of the weather station are listed in Table 1.

As three important sections of the ballastless track-bridge structure with a 32 m span simply-supported box girder, a beam end section (Beam End), a mid-span section (Mid Span) section and a wide-narrow joint at mid-span (WN Joint) are selected to measure their internal temperature distribution. The distance between the WN Joint and the Mid Span is 36 m, and the distance between the Mid-span and the Beam End is 16 m. The ballastless track consists of multi-layer components in the vertical direction, in which two interfaces between the track slab and CA mortar, the CA mortar and base plate are two important parts of heat conduction. Thus, the bottom of the rack slab and base plate are selected as the measuring locations. As shown in Figs. 2(c)-(e), the thermistor thermometer sensors were embedded in the longitudinal slab tracks with 11 sensors in total, since another thermometer sensor was installed at the surface of the bridge to measure the surface temperature. It should be noted that No.7 is installed on the bridge nearby the slab to collect the ambient temperature and three temperature sensors was arranged at the bottom of the track slab, at the middle and bottom of the base plate for three locations, respectively. The wireless temperature data loggers of NT78-Li-C50 from Minden Electronics Technology manufacturer were used to record the real-time, remote, and continuous data from the field. Furthermore, the sensor has a measurement range of -30℃ to +120℃, and a resolution ratio of 0.1℃ to measure the internal temperature of the track-bridge structure. In addition, the collection time of these meteorological factors and internal temperature also started from January 1th 2021 to August 30th 2022 at the same time. Both the sampling frequency of meteorological factors and internal temperature are collected at an interval of 10 minutes through wireless data loggers.

2.2 Neural network architectures

2.2.1 Testing cases of the prediction methods

In internal temperature prediction of the track structure, meteorological parameters are adopted as the input parameters of testing cases, and the internal temperature is used as output parameters. As listed in Table 2, five testing cases for temperature prediction are selected to analyze the impact of different meteorological conditions on internal temperature prediction. Since the ambient temperature has a strong correlation with the internal temperature, the ambient temperature is the mandatory input parameter in five cases. There are 15000 groups of monitoring datasets for every meteorological parameter and corresponding track plate temperature measured from January 2021 to August 2022 were enrolled, of which 70% random data were selected as the training model samples and 30% data were used to validate the training results. All the raw datasets were normalized before the model training. To verify the feasibility of these predicted models, all parameters are used in the internal temperature dataset in the fifth case, and the simulation experiment was carried out on the software Anaconda by using Python 3.9. The model calculation times of five cases will also be recorded.

The evaluation metrics are often utilized to assess the performance of deep learning methods in terms of accuracy and reliability. For example, the Root Means Square Error (RMSE) presents the accuracy of predicted values (Eq. (1)). It uses the same dimension and describes the relationship between the predicted and actual values. Different from RMSE, Mean Absolute Error (MAE) is the average of the absolute difference. It is a real error, which is less impacted by the outliers than RMSE. R2 is equal to 1 - MSE (model)/ MSE (Baseline model). The evaluation criteria of RMSE, MAE and R^2 are selected to comprehensively describe the accuracy of different prediction methods. When the RMSE and MAE are smaller, and the R2 is close to 1, which show that the predict accuracy of the testing cases is better.

$$RMSE = \sqrt{\frac{1}{N}\sum_{i=1}^{N}\left(y_{pi} - y_i\right)^2} \tag{1}$$

$$MAE = \frac{1}{N}\sum_{i=1}^{N}\left(y_{pi} - y_i\right) \tag{2}$$

Table 2 Five testing cases of temperature prediction with various input combinations

Case number	Ambient temperature	Wind speed	Solar radiation	Humidity	Internal temperature
Case 1	√				√
Case2	√	√			√
Case3	√		√		√
Case4	√			√	√
Case5	√	√	√	√	√

$$R^2 = 1 - \frac{\sum_{i=1}^{N}(y_{pi} - y_i)^2}{\sum_{i=1}^{N}(y_i - \bar{y})^2} \quad (3)$$

where N is the quantity of monitoring data, y_{pi} is the i[th] predicted values, $\bar{y}$ is the mean of actual values, and y is the actual value.

2.2.2 Temperature prediction effect by the ANN model

The artificial neural network (ANN) model has been used for a wide range of predict applications in recent years. Since the ANN technique does not require any mathematical knowledge of the input parameters and is able to provide a more effective solution for a variety of problems (Joseph Manoj *et al*. 2019, Meenal and Selvakumar 2018). The ANN is consisting of various neurons and establishes the structure based on the logical-mathematical structure. It stimulates the changeable weight correlation between various neurons and input, hidden, and output layers. Fig. 3(a) shows a typical ANN structure to predict the internal temperature in longitudinal slab tracks under experimental case 5 with consideration of four meteorological factors. An input layer, different fully connected layers, and an output layer are the main structure of a multi-dimension ANN model, in which each hiddenlayer has a number of 50 neurons.

2.2.3 Temperature prediction effect by the LSTM model

The recurrent neural networks (RNN) have a critical difference in the transformer, convolutional, and feedforward architecture. It added a series of undefinable number hidden layers and included various deep recurrent networks with considering the learning architectures. LSTM model is a typical RNN, which could effectively solve the time series data gradient vanishing and long-term dependency. Unlike other RNN models, LSTM uses long-term memory results by considering the backpropagation neural network (Cossu *et al*. 2021). Thus, it could model time series, and the outputs of these series depend on the minimize the training error and various layers (Zhang *et al*. 2020b). Fig. 3(b) is a typical structure of the LSTM model to predict the internal temperature in longitudinal slab

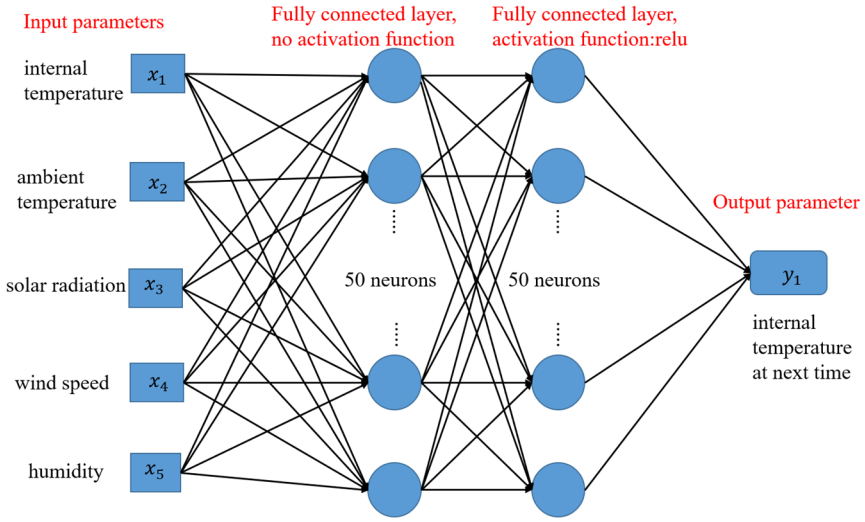

(a)

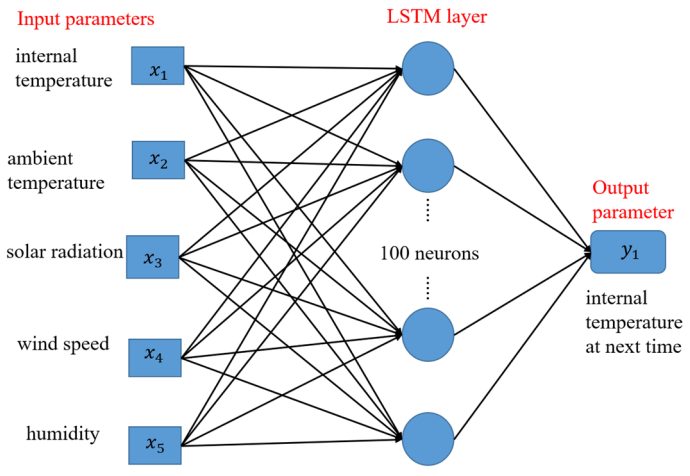

(b)

Fig. 3 Mapping model for five input parameters. (a) ANN; (b) LSTM; (c) CNN

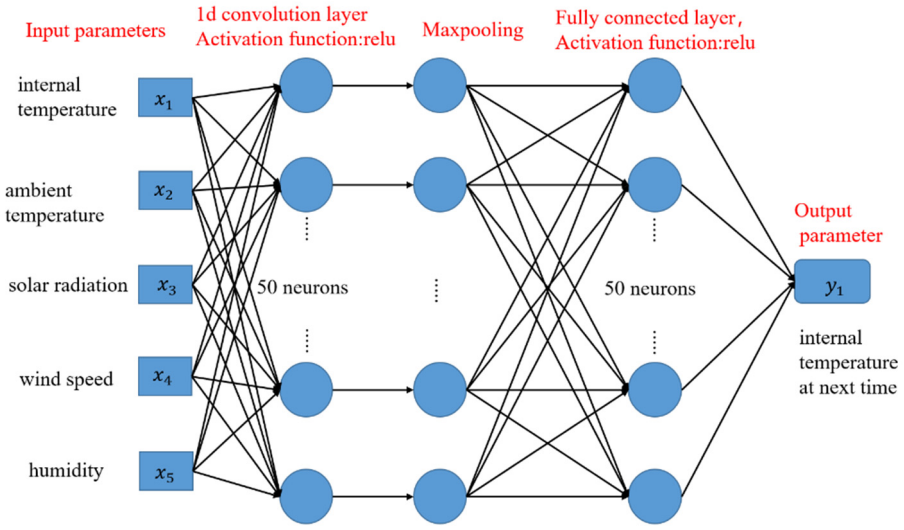

(c)

Fig. 3 Continued

tracks under experimental case 5 with consideration of four meteorological factors. An input layer, an LSTM layer with 100 neurons, and an output layer are the main structure of a LSTM model.

2.2.4 Temperature prediction effect by the CNN model

CNN is a typical feed-forward neural network, which is fully considering sparse connectivity, shared weight, and feature extraction. The characteristics of convolutional networks owe the matrix multiplications enrolling in the convolution neural network (Lee *et al*. 2020). Fig. 3(c) is a typical structure of the CNN model to predict the internal temperature in longitudinal slab tracks under experimental case 5 with consideration of four meteorological factors. In this paper, we selected the CNN model with mainly consists of meteorological parameters series, fully connected layers (no activation function, relu activation function), and output parameters. The 1d convolutional layer employs the Rectified Linear Unit to feature extraction for meteorological parameters, which has 50 neurons in every layer. The meteorological input parameters were enrolled with the neural network model trained, and increased the efficiency of the training function within the hidden layer.

3. Results of meteorological and temperature measurement

3.1 Characteristics of four meteorological factors

The time-dependent variations of four meteorological factors with AT, SR, RH, and WS are the key influential factors of internal temperature prediction in the track structure. The monitoring data of the above four meteorological factors are observed in 18 months, with a total of 55000 data for every meteorological factor. In the data pre-processing, we separated the ambient temperature into the winter with low temperature and the summer with high temperature. As an example, Fig.4 describes the characteristics of these four meteorological factors under the winter period from January 17th to 24th 2021, and the summer period from August 1th to 8th 2022, respectively. The ambient temperature increases to the maximum at the daily maximum temperature plateau from 12:00 AM and 4:00 PM and then decreases from 7:00 pm to 11:00 pm. The minimum temperature was -5℃ on the night of January 17th, while the maximum temperature was 39℃ in the midday of August 1th. Moreover, the average temperature of the winter and summer periods are about 6℃ and 32℃, respectively. Solar radiation continuously rises from 8:00 am to 1:00 pm with the maximum values close around 1:00 pm, while its value approaches zero during the night hours. The maximum value of solar radiation is about 640 W/m^2 at the midday of January 19th and about 1250 W/m^2 at the midday of J August 6th. It should be noted that the large solar radiation was recorded on all sunny days, and some random outliers were noticed on cloudy or rainfall days. There are existing a synchronization between the ambient temperature and solar radiation, the times of the extreme ambient temperatures are close to those of the extreme solar radiation. The wind rose diagrams show that the maximum wind speed during the winter and summary are different. It shows that summer has a stronger wind speed than winter. Also, the wind direction has great change during summer, especially for the southwest (WS) and Northwest (WN) directions. In addition, the maximum and minimum of the relative humidity during these days are about 100% and 11.6%, respectively. The average value of the relative humidity during the winter days and summer days are 56.5 % and 75.6%, respectively. Thus, the climate condition in summer is high temperature and humidity.

3.2 Characteristics of internal temperature at three locations

In the measurement data in 18 months from January 2021 to June 2022, the minimum and maximum value of

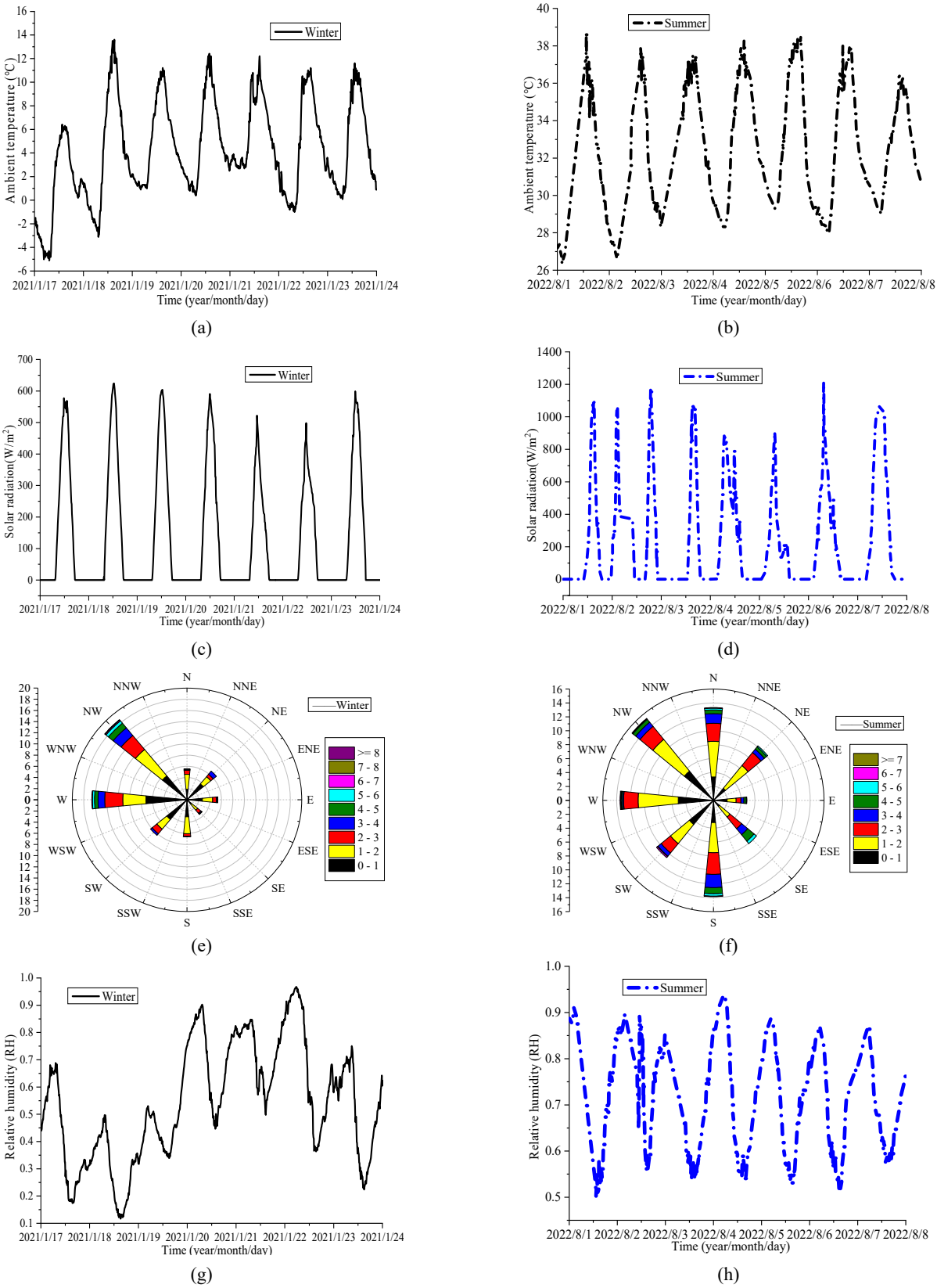

Fig. 4 The characteristics of four meteorological parameters under the winter and summer.
(a)-(b) Ambient temperature; (b)-(c) Solar radiation; (d) Wind rose diagram; (e)-(f) Relative humidity

ambient temperature are 17th January 2021 and 01th August 2022, as illustrated in Figs. 5(a)-(d). During the winter day from 5 am to 12 pm on 17th January, the surface temperature has first slowly increasing before about 8 am, and the internal temperatures of the track slab and base plate rapidly increase after about 10 am with the surface temperature

near the most rapid increasing after 8 am. Then, the internal temperatures of the track slab and base plate gradually decrease after 4 pm with the surface temperature decreasing after about 4 pm. For example, the maximum and minimum values of No. 3 at the beam end on the day are about 6℃ at 4 pm and -2℃ at 3 am, respectively. Most of the internal temperatures of the track slab and base plate ranging from -2℃ to 10℃ are smaller than those of the surface temperature during the daytime. Meanwhile, the internal temperature at the bottom of the track slab (e.g., No.3, No.6, No.10) is slightly larger than the center of the base plate (e.g., No.2, No.5, No.9), while they are much larger than at the bottom of the base plate (e.g., No.1, No.4, No.8). For instance, the peak values at the center and bottom of the base plate (No.2 and No.1) reaches about 4.5℃ and 2℃, respectively. Among three locations, the internal temperature at the mid-span is the smallest while the temperature at the beam end is the largest.

During the summer day from 0 am to 12 pm of 01th August, the internal temperatures of the track slab and base plate firstly decrease to the minimum values at 8 am and then increase to the peak values at about 4 pm, and finally gradually decrease at the night. For example, the maximum

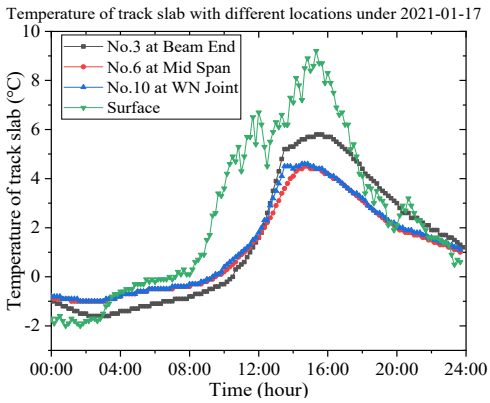

(a)

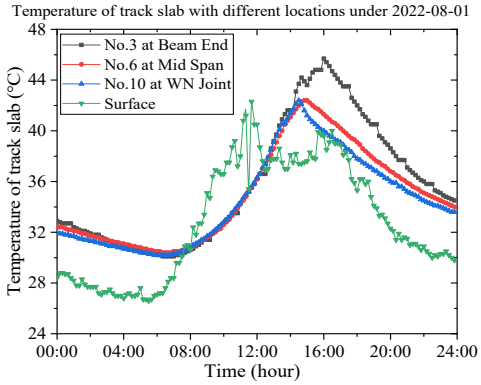

(c)

Fig. 5 The temperature distribution in track structure and Correlation
(a) track slab temperature records at the minimum temperature
(c) track slab temperature records at the maximum temperature
maximum temperature day. (e)-(g) the fitting equation between
of track slab at mid-span, beam end, and wide-narrow joint; (h)
during summer of AT, SR, and WS; (i) oblique plane with three
WS; (j) correlation coefficients with AT, SR, WS, and RH

and minimum values of No.3 at the beam end on the day are about 46℃ at 4 pm and 30℃ at 7 am, respectively. The phenomenon of time lag was obvious compared with the surface temperature and internal temperatures, and the internal temperature during the daytime was larger than the surface temperature. Interestingly, the peak values at the center and bottom of the base plate (No.2 and No.1) reach about 42.5℃ and 34.5℃, respectively. Both the temperature values at the bottom of the track slab and the center of the base plate are larger than those at the bottom of the base plate. Besides, the internal temperature at the beam end of the bridge is also the largest, which is slightly larger than those of the two midspan locations. Thus, the temperature gradient in the vertical direction of the track structure could be appeared due to the daily temperature change, especially at the beam end of the bridge.

3.3 Correlation relationship among four meteorological factors

As shown in Fig. 5(e), the relationships between ambient temperature and internal temperature of the track slab at three locations are an exponential function with the

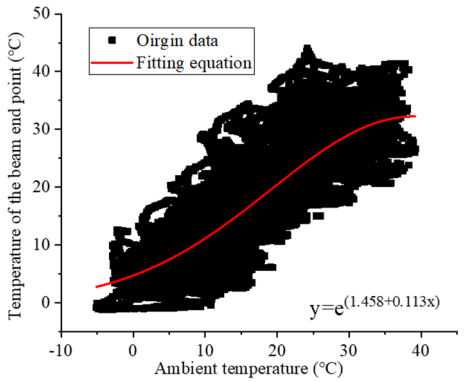

(e)

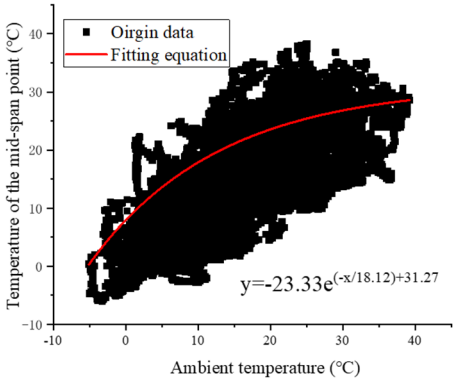

(f)

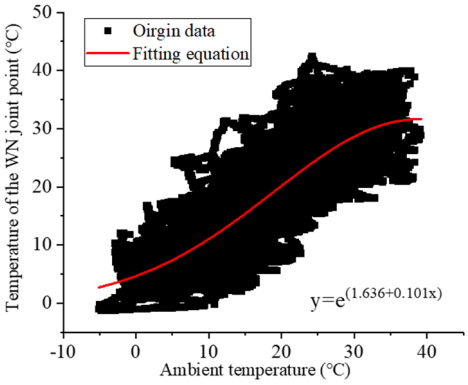

(g)

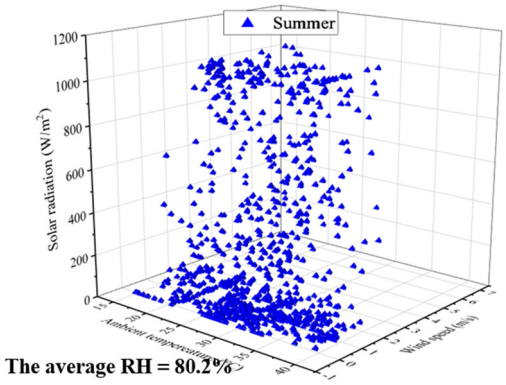

(h)

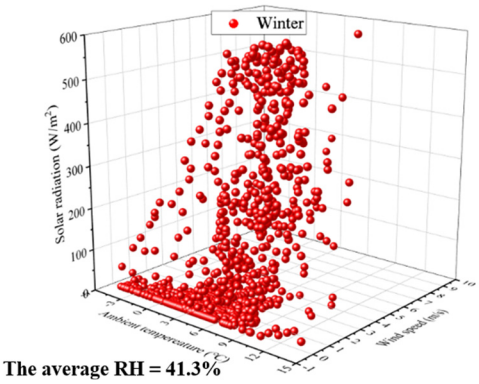

(i)

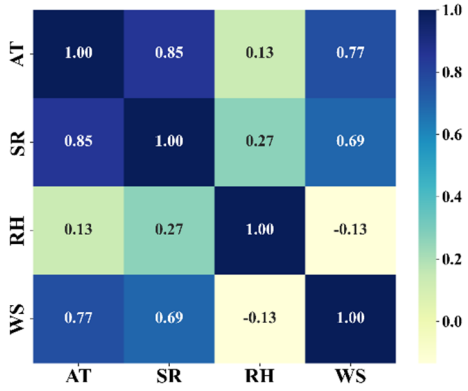

(j)

Fig. 5 Continued

Eqs. (4)-(6) with the best fitting determination coefficients of $R^2 = 0.98$ as follows.

$$y = -23.326\, e^{-\frac{x}{18.12}+31.27} \quad \text{at the mid-span} \tag{4}$$

$$y = e^{1.458-013x} \quad \text{at the beam end} \tag{5}$$

$$y = e^{1.636+-0.099x} \quad \text{at the wide-narrow joint} \tag{6}$$

Where x and y are the ambient and internal temperature, respectively. The internal temperature of the track slab at three locations presents a nonlinear increment as the increase of the ambient temperature, and the relationships have small differences at the three locations.

Three-dimensional relationship among the AT, WS, and SR under the summer and winter are illustrated in Figs. 5(f)-(g), respectively. The oblique plane is observed in the three-dimensional diagram, which indicates there are existing correlation among AT, WS, and SR factors to some extent. In the winter, the range of the AT, WS, and SR belong to -4.5-13.5°C, 0-10 m/s^{2,} and 0-600 W/m^2, respectively. In the summer, the AT, WS, and SR range from 14.5-40°C, 1-7 m/s^2, and 0-1200 W/m^2, respectively. The characteristics of AT, SR, and WS in the oblique plane could reflect the effects of heat conduction, heat radiation, and heat convection of the slab track, respectively. Their correlation relationship in different seasons is helpful to understand the prediction performance of different factors.

The Pearson correlation coefficient is used to evaluate the linear correlation of two data sets of normal continuous

variables (Zhou *et al*. 2016). X,Y represents the sample which contains n sample values ($x_1, x_2, \dots, x_n$) and $(y_1, y_2, y_3, \dots, y_n)$. Eq. (5) is used to calculate the Pearson correlation coefficient.

$$\rho = \frac{(N\sum x_i y_i - \sum x_i y_i)}{\sqrt{Nx_i^2 - (\sum x_i)^2}\sqrt{Ny_i^2 - (\sum y_i)^2}} \quad (7)$$

Here, the value of ρ belongs to [−1, 1]. It shows that ρ closer to 1 represents the positive correlation of X and Y. Also, the ρ closer to −1, it means the X and Y are negative correlations. If the ρ = 0, the linear correlation between X and Y is independent.

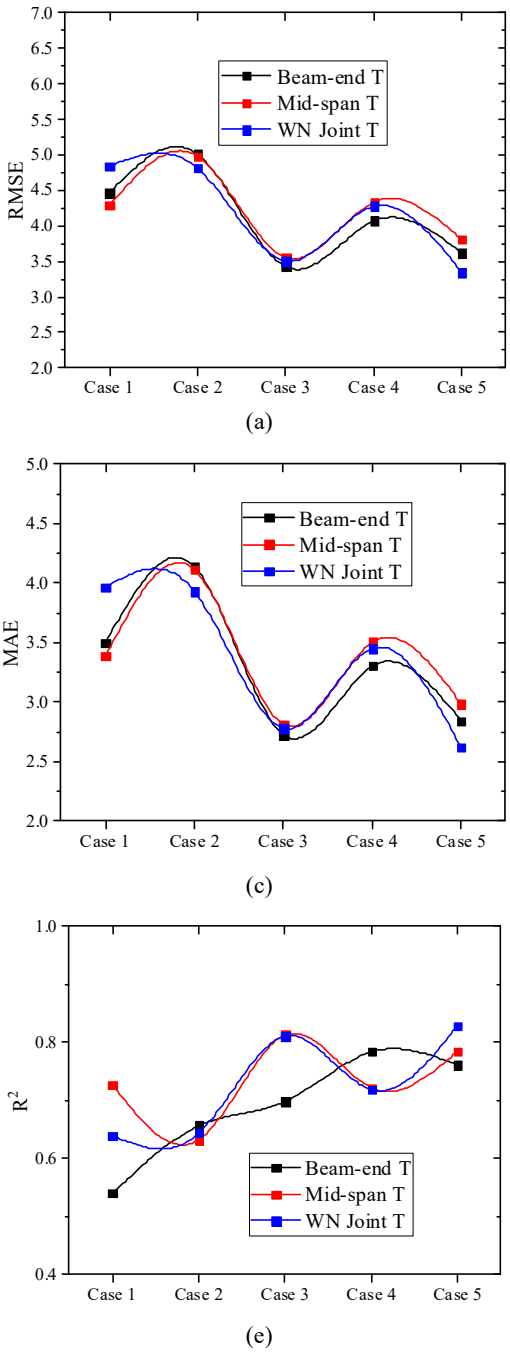

Fig. 6 The ANN prediction results of the Track slab (T) and Base-p
(a)-(b) RMSE result; (c)-(d) MAE result; (e)-(f) R^2 result

With considering the Pearson values, the correlation relationship among the four meteorological factors with AT, SR, RH, and WS is further studied. Fig. 5(h) shows that the correlation coefficient between the AT and SR is the largest with the ρ = 0.85, followed by the correlation coefficient of ρ = 0.77 between the AT and WS, while the correlation coefficient between the AT and RH is very small with the ρ = 0.13. It shows that humidity is a relative independence factor. In conclusion, three meteorological parameters (e.g., AT, WS, SR) have strong correlation relevance, which is selected to the input parameters of internal temperature prediction in longitudinal slab track.

4. Results of various neural network architectures

4.1 Temperature prediction effects of three locations

4.1.1 Results of the ANN model

Fig. 6 compares the predicted results of three indicators (e.g., RMSE, MAE, and R^2) at three locations of the ballastless track-bridge structures under five testing cases based on the ANN model. It should be noted that the 'T' and 'B' represent the sensor installed in the longitudinal track slab and base plate. As for the predict results of track slab, their RMSE and MAE for the three locations are close to each other, and most of the R^2 value at the mid-span in the track slab is slightly larger than that at the beam end. As for the base plate, the RMSE and MAE in the base plate at the WN Joint are much larger than those of two other locations at case 2. Furthermore, the R^2 value in the base plate at the mid-span of the bridge is the highest, whereas the R^2 value in the base plate at the WN Joint of the bridge is the smallest except in case 1. Both the RMSE and MAE of their values of case 5 are the smallest, followed by case 3

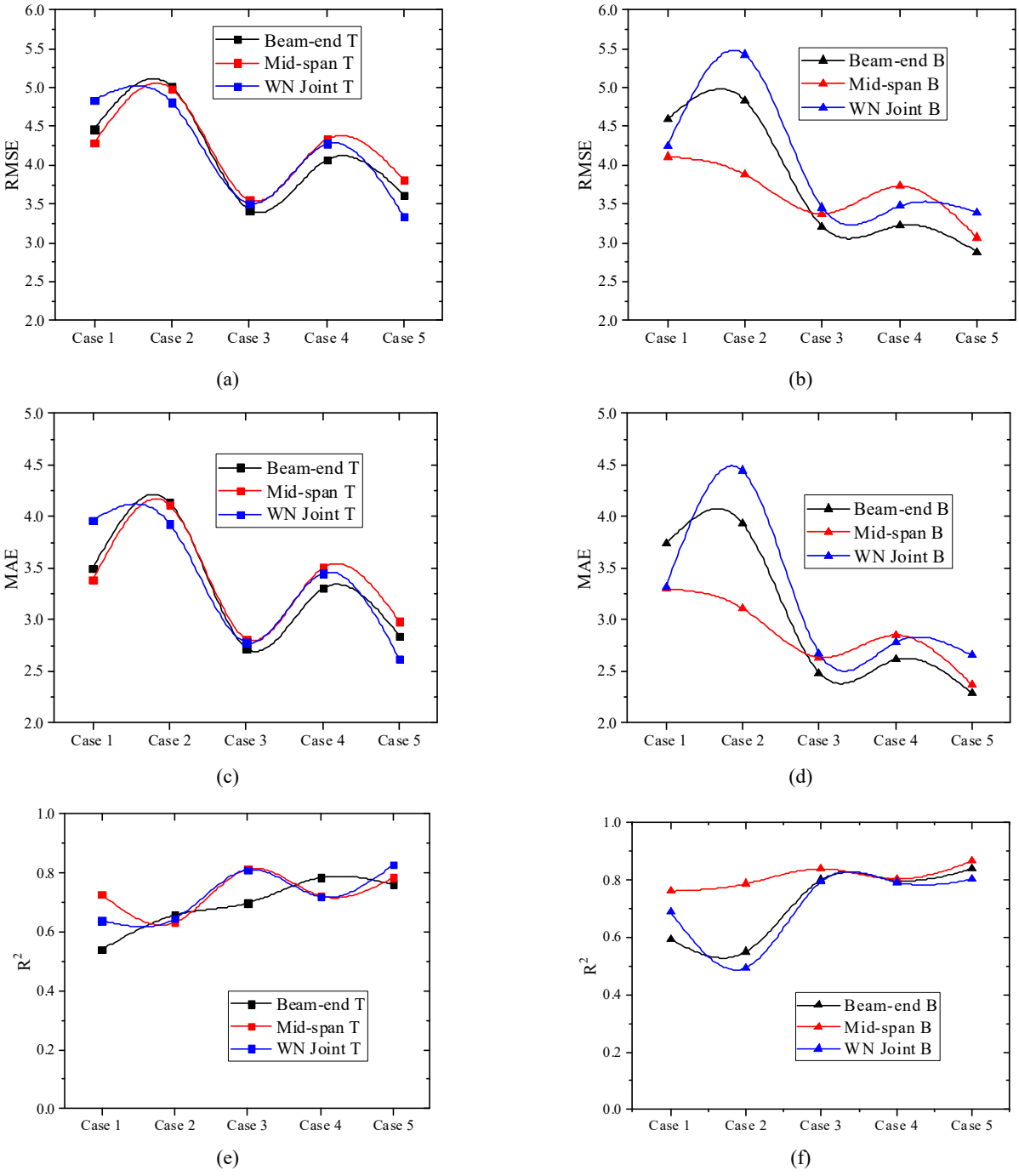

Fig. 7 The LSTM prediction results of Track slab (T) and Base-plate (B) in three locations under five testing cases. (a)-(b) RMSE result; (c)-(d) MAE result; (e)-(f) R^2 result

and case 2 are the largest. The R^2 values of case 3 are close to those of case 5, and the R^2 values of case 2 are the smallest, respectively. The predicted effects of four factors together and only the wind speed as the input parameters are the best and the worst, respectively. It is noted that the predicted effect of only solar radiation on the internal temperature could be easily identified from case 3 as the input parameter. As a consequence, the ANN model in the base plate has the best and the worst accuracy at the mid-span location and the WN Joint, respectively.

4.1.2 Results of the LSTM model

The predicted results of indicators RMSE, MAE, and R^2 in three locations of the track-bridge structures under the five testing cases are also compared based on the LSTM model. Fig. 7 indicates that the RMSE, MAE, and R^2 values of the track slab at three locations are also close to each other, in which the R^2 value at the WN Joint of the track slab is slightly larger than that at the mid-span. It is noted that the RMSE and MAE in the base plate at the WN Joint are much larger than those of two other locations. The R^2 value in the base plate at the mid-span of the bridge is the largest, whereas the R^2 value in the base plate at the WN Joint of the track slab is the smallest. Therefore, the LSTM model has the best and the worst prediction accuracy at the mid-span and the WN Joint location in the longitudinal slab

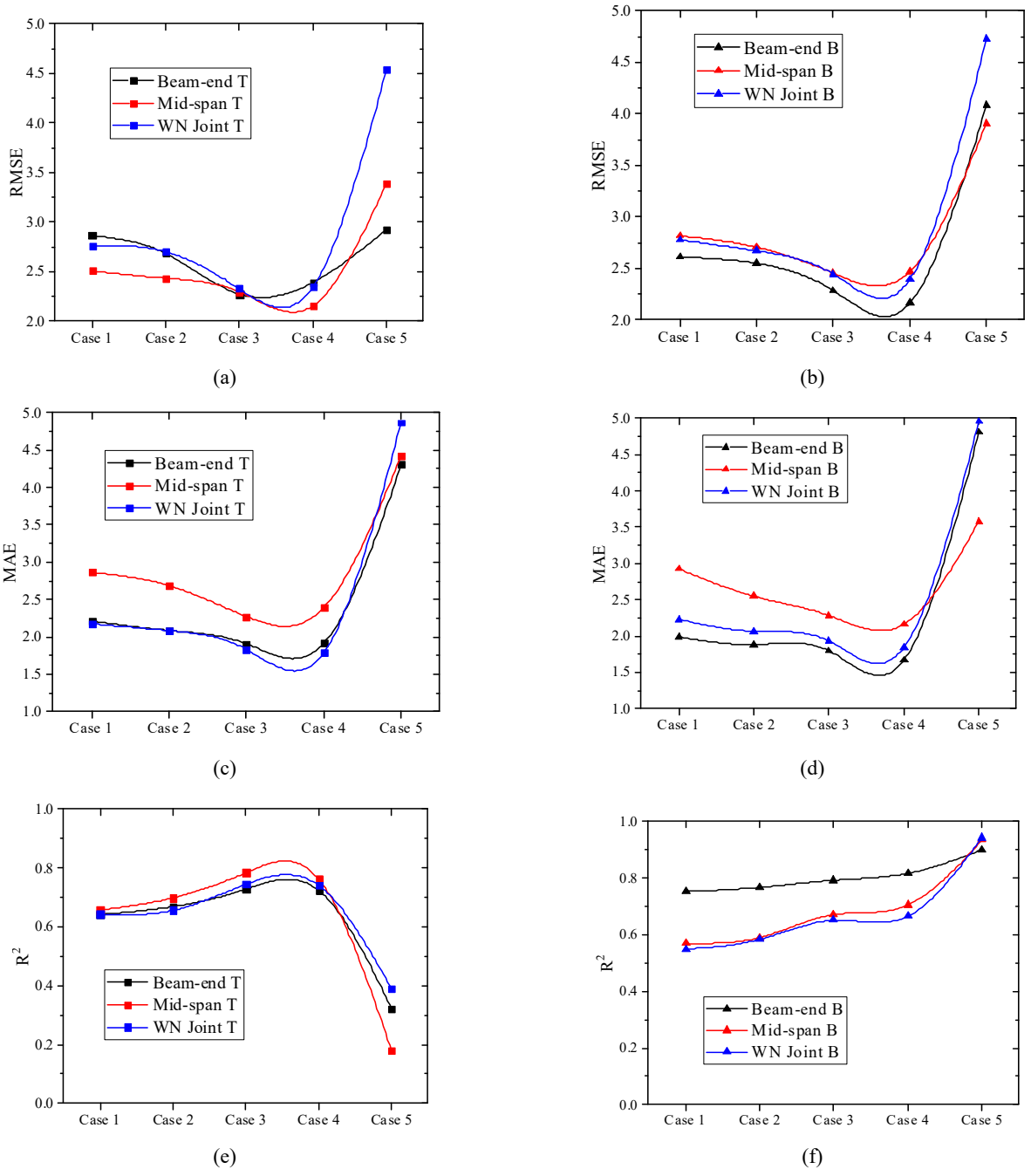

Fig. 8 The CNN prediction results of Track slab (T) and Base-plate (B) in three locations under five testing cases. (a)-(b) RMSE result; (c)-(d) MAE result; (e)-(f) R^2 result

track, respectively.

4.1.3 Results of the CNN model

The predicted results of indicators RMSE, MAE, and R^2 in three locations of the track-bridge structures under the five testing cases are also compared based on the CNN model. Fig. 8 illustrates that the RMSE of the track slab at the mid-span is the smallest, whereas the RMSE of the base plate at the beam end is the smallest among the three locations. Interestingly, both the MAE of the track slab and base plate at the mid-span are the largest. The R^2 value in the track slab at the mid-span of the bridge is the largest, while the R^2 value in the base plate at the beam end is the largest. As a result, the predicted accuracy of the CNN model has the best effect for the track slab at the mid-span location and in the base plate at the beam end of the bridge, respectively.

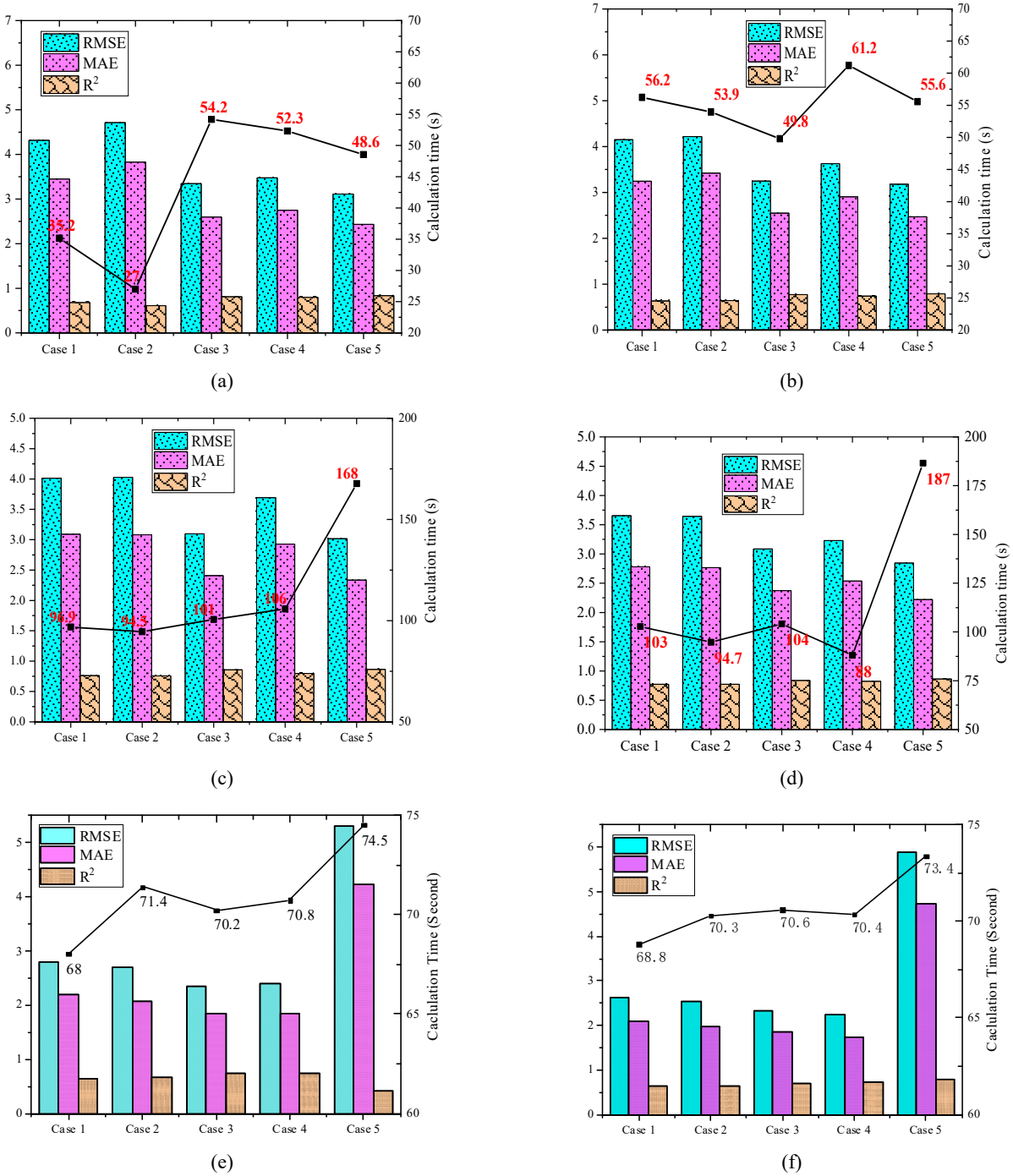

Fig. 9 The indicators of RMSE, MAE, R^2, and calculation time comparison from ANN trained under five experimental cases. (a) ANN track slab; (b) ANN base plate; (c) LSTM track slab; (b) LSTM base plate; (e) CNN track slab; (f) CNN base plate

4.2 Temperature prediction effects of meteorological parameters

4.2.1 Results of the ANN model

Figs. 9(a)-(b) shows the average indicators values (e.g., Calculation time, RMSE, MAE, and R^2) of three locations under five cases in the ANN prediction model. In particular, the RMSE and MAE of case 5 in the track slab and base plate are the smallest among the five cases, followed by case 3, and the RMSE and MAE of case 2 are the largest. In addition, the R^2 value of case 5 in the track structure reaches the largest value of about 0.8, and the R^2 value of case 2 in the base plate is the smallest value of about 0.5. The R^2 value of case 4 in the track slab and base plate is still larger than those of case 1. Nevertheless, the calculation time of case 2 of the track slab is much smaller than in other cases, and the calculation time of case 2 of the base plate is slightly smaller than in other cases. Thus, the prediction accuracy of the wind speed as the input parameter is the worst, and the predicted effect of the humidity is also poor. The predicted accuracy is improved after considering solar radiation as the input parameter, and thus the ANN predict model could effectively the internal temperature in the longitudinal slab track structure.

4.2.2 Results of the LSTM model

The average indicator values of the Calculation time, RMSE, MAE, and R^2 in the track slab and base plate in the LSTM prediction model are also compared in Figs. 9(c)-(d). Although the RMSE and MAE of case 5 are slightly smaller than those of case 3 in the track slab, both the RMSE and MAE values of case 1 are close to those of case 2. As for the internal temperature in the track slab under five cases, the R^2 value of case 5 is close to those of four other cases, while the calculation time of case 5 is much larger than those of four other cases. Likewise, the RMSE and MAE of case 5 and case 3 in the base plate are much smaller than those of case 1 and case 2. The R^2 values in the base plate of five cases are about 0.75, which are also close to those of the track slab. Both the predicted accuracy of the LSTM model without and with the wind speed as the input parameter is the worst, whereas the predicted accuracy is the best when solar radiation is selected as the input parameter. In addition, the calculated time of case 5 in the base plate is also much larger than those of four other cases, but the LSTM in the base-plate structure needs to cost extra time (11%) to get better results. As a result, the LSTM model also effectively predicts the internal temperature in the longitudinal slab track structure, in which the predicted

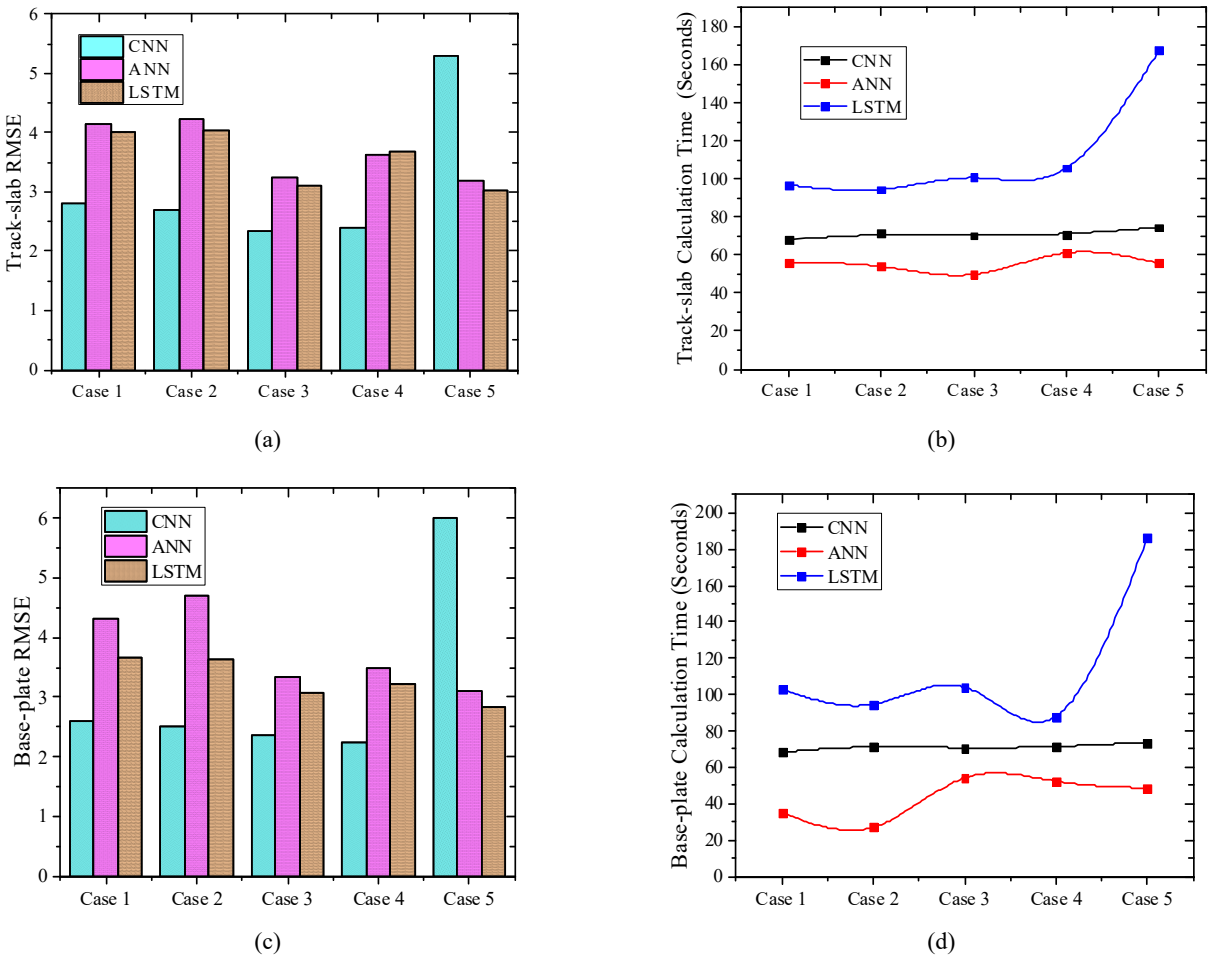

Fig. 10 The average predict results comparison among three models under five testing cases. (a) Average RMSE results in track slab; (b) Average Calculation time in track slab; (c) Average RMSE in the base plate; (d) Average calculation time results in the base plate

accuracy of the LSTM model when four meteorological factors (Case 5) are selected as the input parameters, especially for solar radiation.

4.2.3 Results of the CNN model

The predicted effects of the internal temperature in the track slab and base plate under five testing cases are further compared in Figs. 9(e)-(f), which includes the average indicator values of Calculation time, RMSE, MAE, and R^2, respectively. As for the internal temperature in the track slab, the RMSE, MAE, and calculation of the time in case 5 are much larger than those of the four other cases. Interestingly, the RMSE of case 4 is close to those of case 3, and the MAE of case 4 is the smallest among the five cases. Although both the RMSE and MAE of case 4 in the track slab are the smallest, the calculated time of case 5 is the largest about 74.5 s. Similarly, all of the RMSE, MAE, and calculated time of case 5 in the base plate is the largest, while the RMSE and MAE of case 4 are slightly smaller than those of the four other cases. Besides, the R^2 value of case 5 is even smaller than 0.5, and the R^2 value of case 4 is the largest. Hence, the average predict accuracy of the CNN model is the worst when four meteorological factors are selected for the input parameters at the same time, which does not agree with the real predicted effect of the meteorological factors in the longitudinal slab track structure. Since the CNN model could lead to the key features are discard and feature over-extracting after considering more and more meteorological factors as the input parameters, which indicates that the CNN model is not suitable to predict the internal temperature in the track structure.

4.3 Temperature prediction effect of three prediction methods

In order to compare the predicted effects of the internal temperature by using the CNN, ANN, and LSTM model, the average indicator values of RMSE, and calculation time are compared, respectively. Fig. 10(a) shows that most of the RMSE values in the track slab by using the CNN model are the smallest except for case 5, and the RMSE values by using the ANN model are slightly larger than those of the LSTM model, except for the case 4. However, the RMSE with case 4 is only higher than 0.1 with LSTM. It could consider it has the same performance in case 4. Fig. 10(b) plots most of the architecture calculation times in the track slab by using the various model, in which the LSTM and ANN are the largest and smallest of five cases, respectively. Furthermore, all of the RMSE values in the base plate by using the ANN model are slightly larger than those by using the LSTM model, especially for case 2. Considering all 5 cases, the MAE values in the base plate also have the same change rules as those of RMSE values. Fig. 10(c) also presents that the RMSE values by using the LSTM model are also slightly larger than those of the ANN model. Besides, all of the calculated times by using the ANN model are smaller than 65 s in every case, while the calculated times by using the LSTM model are much higher than those of the LSTM model and ANN model (Fig. 10(d)). In summary, the LSTM model shows the best prediction accuracy in the track slab and base plate under considering four meteorological factors, and the prediction accuracy of four meteorological factors as the input parameters is worse than that of the input parameter with a single meteorological factor for the CNN model. Notably, the calculation time by the LSTM is longer than those of ANN and CNN architectures (save 67% compare with LSTM, save 43% compare with CNN).

5. Conclusions

This paper systematically compares the predicted effects of the internal temperature of three locations by using the ANN, LSTM, and CNN models, through the field-measured platform of four meteorological factors and internal temperatures in track-bridge structures. The major conclusions are summarized as follows:

- In the 18 months, the correlation coefficient between the ambient temperature (AT) and solar radiation (SR) is the largest, and the influence of the four meteorological factors (AT, SR, WS, RH) on the internal temperature predict in the track structure successively becomes smaller.
- The predicted accuracy at the mid-span location by using the ANN and LSTM model is close to two other locations. Both the ANN and LSTM model have the best and worst prediction accuracy in the base plate at the mid-span and WN Joint locations, respectively.
- The predicted effect is the best when the four meteorological factors are input parameters, and the predicted effect of the solar radiation on the internal temperature could be easily identified by using the ANN and LSTM model.
- The LSTM model shows the best prediction accuracy in the temperature field prediction, while the ANN model has a higher computing efficiency and the CNN model is not suitable to predict the internal temperature under four meteorological factors.

Three basic deep-learning methods are implemented to predict the internal temperature of three locations in longitudinal track structures under various meteorological conditions. More and more regional and deep learning methods of field tests will be used to improve the prediction approach in further studies. Also, besides the meteorological factors, the accuracy of prediction could also be influenced by geographical factors, material factors and etc. It still needs further consideration of other external/internal impact factors. The last, finite element analysis of the heat conduction process will also be combined to reveal the mechanism of the temperature load effects in the longitudinal track structure.

Data availability

The data used to support the findings of this study are available from the corresponding author upon request.

Conflicts of interest

The authors declare no potential conflicts of interest with respect to the research, authorship, and/or publications of this article.

Author contributions

Liu, H.L. and Yuan, W.H.: conceptualization, writing—original draft preparation. Zhou, R.: visualization and investigation. Du, Y.L. and Xu, J.M.: methodology, data curation. Chen R: supervision. All authors have read and agreed to the published version of the manuscript.

Acknowledgments

The authors gratefully acknowledge support from the National Key Technologies Research and Development Program "Transportation Infrastructure" "Reveal the list and take command" project (No.2022YFB2603301), National Natural Science Foundation (No. 52278311 and 52008264), the Shenzhen Science and Technology Program under the grant (Nos. GJHZ20220913143006012, GJHZ20200731095802007 and KQTD20180412181337494), Guizhou University talentproject [2022]68, in part by the Foundation of Key L aboratory of Large Structure Health Monitoring and Control in Hebei Province under Grant KLLSHMC2108,MOE Key Laboratory of High-Speed, Railway Engineering,Southwest Jiaotong University: 2021 Open Fund, the Ministry of Education. the Project of Science and t echnology research and development of China RailwayCo., Ltd (No. K2022G038) and the Guangdong Province Natural Science Foundation (No. 2023A1515030148 and 2022A1515010665).

References

Cai, X.P., Luo, B.C., Zhong, Y.L., Zhang, Y.R. and Hou, B.W. (2019), "Arching mechanism of the slab joints in CRTSII slab track under high temperature conditions", *Eng. Fail. Anal*., **98**, 95-108. https://doi.org/10.1016/j.engfailanal.2019.01.076

Cossu, A., Carta, A., Lomonaco, V. and Bacciu, D. (2021), "Continual learning for recurrent neural networks: an empirical evaluation", *Neural Netw*., **143**, 607-627. https://doi.org/10.1016/j.neunet.2021.07.021

Dai, G. and Su, M. (2016), "Full-scale field experimental investigation on the interfacial shear capacity of continuous slab track structure", *Arch. Civil Mech. Eng*., **16**(3), 485-493. https://doi.org/10.1016/j.acme.2016.03.005

Dai, G., Tang, Y., Liang, J., Yang, L. and Chen, Y.F. (2018), "Temperature monitoring of high-speed railway bridges in mountainous areas", *Struct. Eng. Int*., **28**(3), 288-295. https://doi.org/10.1080/10168664.2018.1464376

Dai, B., Frusque, G., Li, Q. and Fink, O. (2022), "Acceleration-Guided Acoustic Signal Denoising Framework Based on Learnable Wavelet Transform Applied to Slab Track Condition Monitoring", *IEEE Sens. J*., **22**(24), 24140-24149. https://doi.org/10.1109/JSEN.2022.3218182

Guo, Y.Q., Li, Z.W., He, Y.L. and Lu, H.Y. (2018), "A novel method of fore-warning the positive temperature gradient of CRTS II ballastless track based on support vector machine", *J. Railway Sci. Eng*., **15**(9), 2209-2216. [In Chinese]

Guo, W., Wang, Y., Zhai, Z. and Du, Q. (2022), "Seismic control of high-speed railway bridge using S-shaped steel damping friction bearing", *Smart Struct. Syst*., *Int. J*., **30**(5), 479-500. https://doi.org/10.12989/sss.2022.30.5.479

Joseph Manoj, R., Anto Praveena, M.D. and Vijayakumar, K. (2019), "An ACO–ANN based feature selection algorithm for big data", *Clust. Comput*., **22**(2), 3953-3960. https://doi.org/10.1007/s10586-018-2550-z

Lee, S., Kim, H., Lieu, Q.X. and Lee, J. (2020), "CNN-based image recognition for topology optimization", *Know Based Syst*., **198**, 105887. https://doi.org/10.1016/j.knosys.2020.105887

Liu, S., Shi, C., Wang, T., Yang, J. and Chen, X. (2023), "Development of a new modified TSRST test to measure the thermal stress of asphalt supporting layer in the slab track system", *Meas*., **207**, 112422. https://doi.org/10.1016/j.measurement.2022.112422

Lou, P., Zhu, J., Dai, G. and Yan, B. (2018), "Experimental study on bridge-track system temperature actions for Chinese high-speed railway", *Arch. Civil Mech. Eng*., **18**, 451-464. https://doi.org/10.1016/j.acme.2017.08.006

Lu, D. and Wang, C. (2023), "Three-dimensional temperature field inversion calculation based on an artificial intelligence algorithm", *Appl. Therm. Eng*., **225**, 120237. https://doi.org/10.1016/j.applthermaleng.2023.120237

Ma, Z. and Gao, L. (2021), "Predicting mechanical state of high-speed railway elevated station track system using a hybrid prediction model", *KSCE J. Civil Eng*., **25**(7), 2474-2486. https://doi.org/10.1007/s12205-021-1307-z

Meenal, R. and Selvakumar, A.I. (2018), "Assessment of SVM, empirical and ANN based solar radiation prediction models with most influencing input parameters", *Renew Energy*, **121**, 324-343. https://doi.org/10.1016/j.renene.2017.12.005

Ren, J., Deng, S., Zhang, K., Du, W. and Wu, Q. (2021), "Design theories and maintenance technologies of slab tracks for high-speed railways in China: a review", *Transport Safety Environ*., 3(4), p. tdab024.

Shi, T., Lou, P., Zheng, W. and Sheng, X. (2022), "A hybrid approach to predict vertical temperature gradient of ballastless track caused by solar radiation", *Constr. Build. Mater*., **352**, 129063. https://doi.org/10.1016/j.conbuildmat.2022.129063

Su, M., Dai, G., Marx, S., Liu, W. and Zhang, S. (2019), "A brief review of developments and challenges for high-speed rail bridges in China and Germany", *Struct. Eng. Int*., **29**(1), 160-166. https://doi.org/10.1080/10168664.2018.1456892

Su, M., Xie, H., Kang, C. and Li, S. (2021), "Determination of the interfacial properties of longitudinal continuous slab track via a field test and ANN-based approaches", *Eng. Struct*., **246**, 113039. https://doi.org/10.1016/j.engstruct.2021.113039

Wang, W., Hu, W., Wang, W., Xu, X., Wang, M., Shi, Y., Qiu, S. and Tutumluer, E. (2021), "Automated crack severity level detection and classification for ballastless track slab using deep convolutional neural network", *Autom. Constr*., **124**, 103484. https://doi.org/10.1016/j.autcon.2020.103484

Xin, X., Ren, Z., Yin, Y. and Gao, J. (2022), "Intelligent identification of mortar void in ballastless slab track using the wheelset acceleration combined with CNN-SVM", *J. Mech. Sci. Technol*., **36**(12), 5845-5857. https://doi.org/10.1007/s12206-022-1103-9

Xu, Q., Sun, S., Xu, Y., Hu, C., Chen, W. and Xu, L. (2022), "Influence of temperature gradient of slab track on the dynamic responses of the train-CRTS III slab track on subgrade nonlinear coupled system", *Sci. Rep*., **12**(1), 14638. https://doi.org/10.1038/s41598-022-18898-y

Yang, R., Li, J., Kang, W., Liu, X. and Cao, S. (2017), "Temperature characteristics analysis of the ballastless track under continuous hot weather", *J. Transp. Eng. A-SYST.*, **143**(9), 04017048. https://doi.org/10.1061/JTEPBS.0000076

Yu, Y., Tang, L., Ling, X., Cai, D., Ye, Y. and Geng, L. (2020), "Mitigation of temperature-induced curling of concrete roadbed along highspeed railway: in situ experiment and numerical simulation", *KSCE J. Civil Eng.*, **24**(4), 1195-1208. https://doi.org/10.1007/s12205-020-0671-4

Zhang, J., Jiang, H., Ding, F., Zhang, P., Zhou, F., Li, T. and Duan, N. (2020a), "Effects of metal-ceramic anticorrosion coating on the performance of ballastless tracks at high temperature", *Arch. Civil Mech. Eng.*, **2**, 120. https://doi.org/10.1007/s43452-020-00123-0

Zhang, R., Liu, Y. and Sun, H. (2020b), "Physics-informed multi-LSTM networks for metamodeling of nonlinear structures", *Comput. Methods Appl. Mech. Eng.*, **369**, 113226. https://doi.org/10.1016/j.cma.2020.113226

Zhang, Q., Dai, G. and Tang, Y. (2022), "Thermal Analysis and Prediction Methods for Temperature Distribution of Slab Track Using Meteorological Data", *Sens.*, **22**(17), 6345. https://doi.org/10.3390/s22176345

Zhao, L., Zhou, L., Yu, Z., Mahunon, A.D., Peng, X. and Zhang, Y. (2021), "Experimental study on CRTS II ballastless track-bridge structural system mechanical fatigue performance", *Eng Struct.*, **244**, 112784. https://doi.org/10.1016/j.engstruct.2021.112784

Zhou, H., Deng, Z., Xia, Y. and Fu, M. (2016), "A new sampling method in particle filter based on Pearson correlation coefficient", Neurocomputing, **216**, 208-215. https://doi.org/10.1016/j.neucom.2016.07.036

Zhou, W.B., Zhang, Y., Jiang, L., Feng, Y., Liu, X. and Lai, Z. (2021), "Critical coupling span number in high-speed railway simply supported beam bridge", *Smart Struct. Syst., Int. J.*, **28**(1), 13-28. https://doi.org/10.12989/sss.2021.28.1.013

Zhou, R., Zhu, X., Huang, J., Zhou, H., Liu, H., Ma, C. and Zhang, L. (2022a), "Structural damage analysis of CRTS II slab track with various interface models under temperature combinations", *Eng. Fail. Anal.*, **134**, 106029. https://doi.org/10.1016/j.engfailanal.2022.106029

Zhou, R., Zhu, X., Ren, W.X., Zhou, Z., Yao, G., Ma, C. and Du, Y. (2022b), "Thermal evolution of CRTS II slab track under various environmental temperatures: Experimental study", *Constr. Build. Mater.*, **325**, 126699. https://doi.org/10.1016/j.conbuildmat.2022.126699

Zhou, R., Yuan, W., Liu, W., Zhu, X., Yao, G., Li, F. and Zhang, L. (2023a), "Thermal performance of CRTS II slab track-bridge structure under extreme temperatures: Numerical simulation", *Constr. Build Mater.*, **377**, 131147. https://doi.org/10.1016/j.conbuildmat.2023.131147

Zhou, R., Yue, H., Du, Y., Yao, G., Liu, W. and Ren, W. (2023b), "Experimental and numerical study on interfacial thermal behavior of CRTS II slab track under continuous high temperatures", *Eng. Struct.*, **284**, 115964. https://doi.org/10.1016/j.engstruct.2023.115964

Zumin, O. and Fujian, L. (2014), "Analysis and prediction of the temperature field based on in-situ measured temperature for CRTS-II ballastless track", *Energy Procedia*, **61**, 1290-1293. https://doi.org/10.1016/j.egypro.2014.11.1083